

Pressure induced solid-solid reconstructive phase transition in LiGaO₂ dominated by elastic strainQiwei Hu,¹ Xiaozhi Yan,² Li Lei,^{1,*} Qiming Wang,¹ Leihao Feng,¹ Lei Qi,¹ Leilei Zhang,¹
Fang Peng,¹ Hiroaki Ohfuji,³ and Duanwei He¹¹*Institute of Atomic and Molecular Physics, Sichuan University, 610065 Chengdu, People's Republic of China*²*Center for High Pressure Science and Technology Advanced Research (HPSTAR), Shanghai 201203, People's Republic of China*³*Geodynamics Research Center, Ehime University, Matsuyama 790-8577, Japan*

(Received 2 November 2017; revised manuscript received 12 January 2018; published 25 January 2018)

Pressure induced solid-solid reconstructive phase transitions for graphite-diamond, and wurtzite-rocksalt in GaN and AlN occur at significantly higher pressure than expected from equilibrium coexistence and their transition paths are always inconsistent with each other. These indicate that the underlying nucleation and growth mechanism in the solid-solid reconstructive phase transitions are poorly understood. Here, we propose an elastic-strain dominated mechanism in a reconstructive phase transition, β -LiGaO₂ to γ -LiGaO₂, based on *in situ* high-pressure angle dispersive x-ray diffraction and single-crystal Raman scattering. This mechanism suggests that the pressure induced solid-solid reconstructive phase transition is neither purely diffusionless nor purely diffusive, as conventionally assumed, but a combination. The large elastic strains are accumulated, with the coherent nucleation, in the early stage of the transition. The elastic strains along the $\langle 100 \rangle$ and $\langle 001 \rangle$ directions are too large to be relaxed by the shear stress, so an intermediate structure emerges reducing the elastic strains and making the transition energetically favorable. At higher pressures, when the elastic strains become small enough to be relaxed, the phase transition to γ -LiGaO₂ begins and the coherent nucleation is substituted with a semicoherent one with Li and Ga atoms disordered.

DOI: [10.1103/PhysRevB.97.014106](https://doi.org/10.1103/PhysRevB.97.014106)**I. INTRODUCTION**

Solid-solid reconstructive phase transitions (PTs) abound in nature. Understanding the underlying nucleation mechanisms of the reconstructive PT at the atomic level is a key topic in designing special function materials [1,2], geoscientific research [3], and diamond synthesis [4,5]. Nevertheless, observing the solid-solid PT *in situ* is a great challenge. In a reconstructive PT, the lack of group-subgroup relation between the phases causes significant strains from the initial to the final phase. Hence *a priori* a preferable way of mapping the positions from the initial structure to the final becomes impossible [6]. Furthermore, the solid-solid PTs are usually accompanied with elastic strains generated by partial lattice misfits between coexisting phases, making it more difficult to exactly calculate the total energy for the phase transition [7,8]. Although several nucleation mechanisms based on different intermediate phases in the PT, wurtzite-rocksalt, were proposed through first-principles calculations [9] and molecular dynamics simulations [10], the underlying nucleation mechanism of the pressure induced solid-solid PT still remains open. For instance, the actual transition pressures for graphite-diamond [4,5,11], wurtzite-rocksalt in GaN [9,12], and AlN [13–15] are significantly higher than the calculated equilibrium coexistence pressure; the transition path in pure GaN passes through a tetragonal metastable configuration, while the wurtzite structure directly transforms to the rocksalt phase at 5% of cation substitution [16]. At low stress or hydrostatic pressure, the wurtzite CdS is transformed to the rocksalt structure passing through a

fivefold-coordinated intermediate structure, and at high stress CdS directly transforms into the rocksalt phase [17]; however, the wurtzitelike γ -LiAlO₂ directly transforms to rocksalt-like δ -LiAlO₂ even at hydrostatic pressure of 3.7 GPa [18]. Stimulated by these open questions, we propose an elastic-strain dominant mechanism in the solid-solid reconstructive PT. Because of the underestimate or neglect of the elastic strains, the calculated transition pressure is much lower than experimental. At low stress, the appearance of the intermediate structure can reduce the elastic strains at the solid-solid phase interface making the transition energetically favorable; at high stress, the external stress can directly relax the elastic strains.

During the pressure induced solid-solid PT, the transformation strain is the main geometric characteristic that transforms the lattice of the parent phase into the product phase [19]. Especially, in reconstructive PT the transformation strains are so large that the product and parent phase can coexist at a large pressure range; meanwhile, the shear stress should be generated if the elastic modulus between the parent and product phase are different [20,21]. In the early stage of the solid-solid PT, the nucleus is often formed via coherent nucleation at the dislocations, where the coherent nucleation happens at lower energy cost [22]. Consequently, large elastic strains are accumulated due to the lattice misfits between the nucleus and the parent phase; i.e., each lattice would be elastically deformed with respect to what it would be when the other phase was absent [20,23,24]. These large elastic strains in turn reduce the driving force for the nucleation [19]. In this case, if the elastic strains can be relaxed by the shear stress generated by transformation strain and/or the external stress, the critical nucleus can be formed and the PT occurs. Therefore, the transition γ -LiAlO₂ to δ -LiAlO₂ occurs even at hydrostatic pressure

*lei@scu.edu.cn

3.7 GPa [18], in good agreement with the calculated one, 3.1 GPa [25], as the elastic strains only along the $\langle 001 \rangle$ direction are small and can be directly relaxed by the internal shear stress generated by the volumetric transformation strain (21%). If the elastic strains are too large to be relaxed, an intermediate structure will emerge and even higher pressure and higher temperature will be required to relax the elastic strains. This situation can be found in the phase transitions of the graphite-diamond [26–28] and the binary semiconductors [12–15]. Additionally, the relaxation mechanism of the elastic strains can not only significantly affect the thermodynamics and kinetics of the solid-solid transformation but also determine the type of microstructure such as dislocation, twinning, and disordering. In this work, we present the *in situ* quasi-hydrostatic and nonhydrostatic compression studies in a ternary wurtzitelike structure, β -LiGaO₂, using angle-dispersive x-ray diffraction (ADXRD) and Raman scattering (RS) techniques at room temperature. Due to the significant elastic strains, β -LiGaO₂ (orthorhombic, space group $Pna2_1$) firstly transforms to an intermediate deformed structure above 8 GPa so as to reduce the elastic strains, and then to γ -LiGaO₂ (tetragonal, space group $I4/m$) at about 11.1 GPa. Finally, the cation-disordering structure grows with further relaxing elastic strains.

II. EXPERIMENTS

High pressure was generated using a symmetric-type diamond-anvil cell (DAC) with 400- μm culets. The homogeneous samples or single-crystal plate were loaded in a 100- μm hole which was drilled in a T301 steel disk indented to about 30 μm thickness. An ethanol-methanol mixture (1:4) and NaCl were used as the pressure transmitting medium for quasi-hydrostatic and nonhydrostatic, respectively. The pressure was determined by the ruby fluorescence method with an error of 0.1 GPa at lower pressure and an error of less than 0.5 GPa at the highest pressure [29]. The ADXRD measurements were performed at the 4W2 beam line of the Beijing Synchrotron Radiation Facility (BSRF, China). A Si (111) monochromator was used to tune the synchrotron source with a wavelength of 0.6199 Å. The incident x-ray beam was focused to approximately $26 \times 8 \mu\text{m}^2$ full width at half maximum (FWHM) spot by a pair of Kirkpatrick-Baez mirrors. The two-dimensional diffraction patterns were taken by a Mar345 image plate detector and analyzed with the program FIT2D [30]. The single-crystal high-pressure Raman scattering experiments were carried out on a custom-built confocal Raman spectrometry system in the backscattering geometry based on triple grating monochromator (Andor Shamrock SR-303i-B, EU) with an attached EMCCD (ANDOR Newton DU970P-UVB, EU), excitation by a solid-state laser at 532 nm (RGB laser system, NovaPro, Germany), and collection by a $20\times$, 0.28 NA objective (Mitutoyo, Japan).

III. RESULTS AND DISCUSSION

A. Structure of β -LiGaO₂ under pressure: ADXRD results

Representative high-pressure ADXRD patterns are shown in Fig. 1(a). During quasi-hydrostatic compression, the starting β -LiGaO₂ phase persists up to 11.1 GPa and several new peaks appear at 11.4 GPa, clearly indicating the onset of a

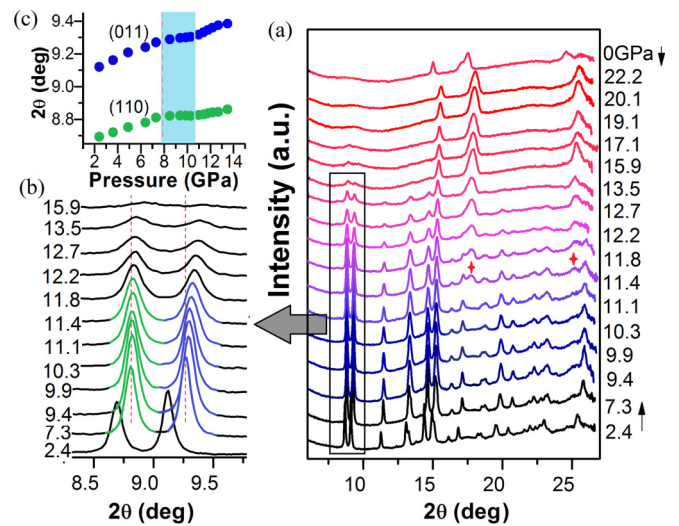


FIG. 1. (a) ADXRD patterns for β -LiGaO₂ at different pressures at room temperature. The red asterisks mark the new peaks of γ -LiGaO₂; (b) detailed ADXRD patterns of the (110) and (011) peaks; (c) pressure dependence of the (110) and (011) peaks' positions.

PT. The transition pressure is much higher than the calculated one, 3.7 GPa [31]. The new peaks dominate the ADXRD spectra at 15.9 GPa, suggesting the completion of the PT. It is worth noting that the two dominated peaks of (110) and (011) exhibit abnormal compressive behaviors at the range of 8–11 GPa [Figs. 1(b) and 1(c)]. With increasing pressure, the (110) plane remains unchanged while the (011) plane shows slight discontinuous compression, indicating that β -LiGaO₂ undergoes structural deformation before PT. The two typical ADXRD patterns at 2.4 and 11 GPa and their Rietveld refinements of both are presented in Fig. 2(a). Both of them can be indexed with the orthorhombic structure (space group $Pna2_1$) [32]. The refined unit-cell parameters for these phases are $a = 5.3687(4)$ Å, $b = 6.3114(5)$ Å, and $c = 4.9562(3)$ Å at 2.4 GPa and $a = 5.2870(8)$ Å, $b = 6.1655(4)$ Å, and $c = 4.8312(8)$ Å at 11.1 GPa. The noticeable pressure induced changes in the relative peak intensities of (110), (011), (210), and (201) are mostly attributed to the variation of the oxygen atom position. All the new diffraction peaks remain after releasing pressure from 22.2 GPa, revealing that the

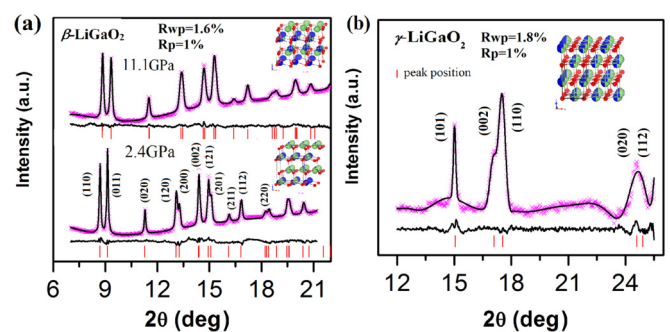


FIG. 2. (a) Rietveld refinements for β -LiGaO₂ at 2.4 and 11.1 GPa, respectively; (b) Rietveld refinement for the quenched γ -LiGaO₂; insets represent the atomic structures.

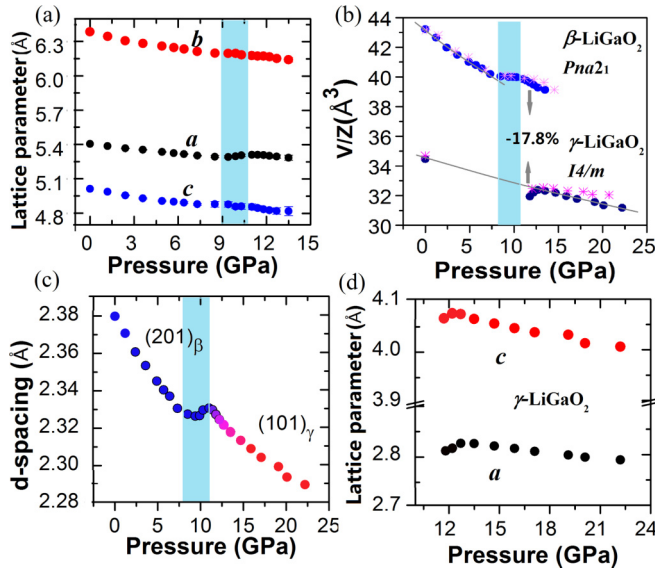


FIG. 3. (a) Pressure-dependent lattice parameters of β -LiGaO₂; (b) volume changes under high pressure for β -LiGaO₂ and γ -LiGaO₂ are fitted to a third-order Birch-Murnaghan equation; the blue dots represent experiments done with an ethanol-methanol mixture (1:4) as the pressure transmitting medium and the red asterisks represent experiments with NaCl; (c) Pressure dependence of d spacing of (201) _{β} and (101) _{γ} ; (d) pressure-dependent lattice parameters of γ -LiGaO₂.

pressure induced PT is irreversible. This high-pressure phase can be indexed with a tetragonal structure, γ -LiGaO₂, with cation disordered (space group $I4/m$) [33,34]. The quenched ADXRD pattern and the Rietveld refinement are presented in Fig. 2(b). The refined unit-cell parameters of γ -LiGaO₂ are $a = 2.8723(3)$ Å and $c = 4.1691(9)$ Å, in good agreement with our previous results in large-volume press experiments [35]. During nonhydrostatic compression, β -LiGaO₂ shows similar behaviors (see the Supplemental Material [36]).

Figure 3 shows the evolution of lattice parameters with increasing pressure. The compression of β -LiGaO₂ is non-isotropic, the a axis being the less compressed and even expanding above 9 GPa [Fig. 3(a)]. Interestingly, at the transition pressures, 11.4–14 GPa, β -LiGaO₂ becomes uncompressible in the a axis while γ -LiGaO₂ shows anomalous expansion both in the a and c axes [Fig. 3(d)]. Figure 3(b) shows the relative unit-cell volumes of both phases as a function of pressure in quasihydrostatic and nonhydrostatic conditions. We analyzed the volume changes in the quasihydrostatic condition using a third-order Birch-Murnaghan equation of state (EOS) in the normal range [37]. The obtained bulk modulus B_0 and its pressure derivative B' for β -LiGaO₂ are 58.3(4) GPa and 4.5(5), respectively. The value of B_0 is well consistent with the value of resonance-antiresonance measurement, 60 GPa [38], and is smaller than the calculated ones, 80 GPa [31] and 95 GPa [39]. The bulk modulus, B_0 , and its pressure derivative, B' , for γ -LiGaO₂ are 127.2(6) GPa and 3.8(3), respectively. The obtained bulk modulus, B_0 , is smaller than the calculated value, 164 GPa [31]. It is worth noting that the volume compression reaches up to 17.8% from β - to γ -LiGaO₂. This large volume change and the big difference in B_0 will

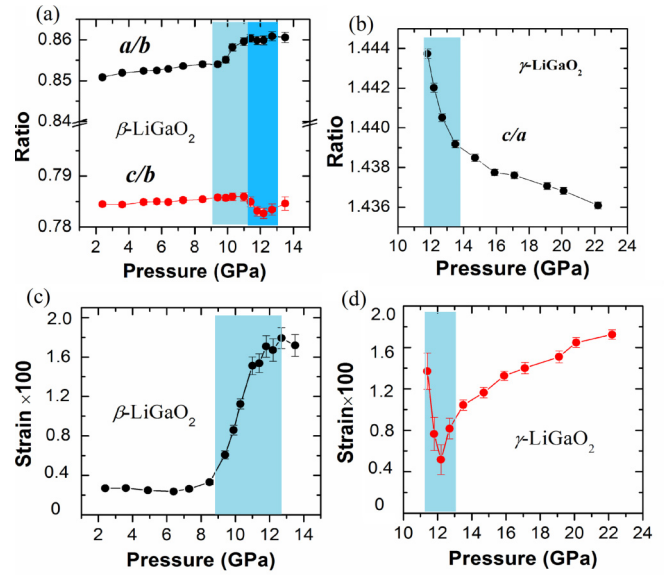


FIG. 4. (a,b) Lattice strains for β -LiGaO₂ and γ -LiGaO₂ with increasing pressure; (c,d) pressure dependence of the microscopic elastic strains for β -LiGaO₂ and γ -LiGaO₂.

generate significant shear stress in the solid-solid interface, which in turn plays an important role in softening the material. Figure 3(c) shows that the (101) plane of γ -LiGaO₂ is coherent with the (201) plane of β -LiGaO₂. Because of the different plane distances, $d(201)_\beta < d(101)_\gamma$, the two planes are subjected to a stress imposed by the other phase. As a result, each phase is elastically deformed with respect to what it would be when the other phase was absent. Thus $d(201)_\beta$ expands while $d(101)_\gamma$ contracts. These elastic strains are magnified in the unit-cell volume.

In Fig. 4, we present the evolution of the lattice strain and the microscopic elastic strains. We specify two lattice strains in the orthorhombic β -LiGaO₂, a/b and c/b , and one lattice strain in the tetragonal γ -LiGaO₂, c/a . The microscopic elastic strains can be derived from the Scherrer equation, deconvoluting grain size and the microscopic strain effect on the diffraction linewidths [40],

$$(2w_{hkl}\cos\theta_{hkl})^2 = \left(\frac{\lambda}{d}\right)^2 + \sigma^2\sin^2\theta_{hkl}, \quad (1)$$

where $2w_{hkl}$ denotes the full width at half maximum (FWHM) on the 2θ scale of the reflection (hkl). The symbols d , λ , and σ denote the grain size, x-ray wavelength, and microscopic strains, respectively.

Before the PT, the two lattice strains increase linearly with increasing pressure. Interestingly, the lattice strain a/b starts to increase steeply at 9 GPa and is locked at 11.1 GPa [Fig. 4(a)]. At this point, we can infer that β -LiGaO₂ is transformed into an intermediate structure by expanding along the $\langle 100 \rangle$ direction. Above 11.1 GPa, the lattice strain c/b shows a drastic decrease, suggesting that the intermediate structure transforms into γ -LiGaO₂ through contraction along the $\langle 001 \rangle$ direction. Meanwhile, huge microscopic elastic strains are generated above 8 GPa [Fig. 4(c)], indicating that the intermediate structure is coherent with β -LiGaO₂. The elastic strains should

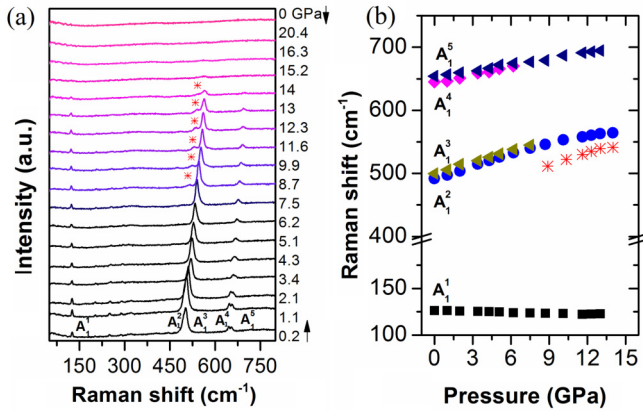


FIG. 5. (a) Typical Raman spectra of β -LiGaO₂ at different pressures. The red asterisks denote the occurrence of the intermediate structure; (b) pressure dependence of the Raman modes in both structures.

be even larger if β -LiGaO₂ directly transforms to γ -LiGaO₂. At the transition pressures, the lattice strain c/a in γ -LiGaO₂ decreases swiftly [Fig. 4(b)], suggesting that the great elastic strains remain in the high-pressure phase and are relaxed by some mechanism. In the energetic crystal [CH₂ – N(NO₂)₄] (HMX), the internal stress generated by the transition strains can cause virtual melting along the interface at the temperature significantly below the melting point [19,41], which leads to release of the internal elastic strains. For β -LiGaO₂, the great transition strains (17.8%) and the significant difference in the bulk modulus should generate significant internal shear stress, which will soften the solid-solid interface and cause the cations to be disordered, and then relax the elastic strains [Fig. 4(d)].

B. High-pressure Raman scattering study of single β -LiGaO₂

The length scales and the time scales of the nucleation process are equivalent to the vibrational frequency of atoms, so *in situ* high-pressure Raman scattering can shed more light on the atomic picture during the PT. In β -LiGaO₂, since 16 atoms exist in the cell, there are 48 modes in total. Removing the zero-frequency pure translation along x , y , or z at the Brillouin-zone center, we can retain the optical modes: $\Gamma = 11A_1 + 12A_2 + 11B_1 + 11B_2$. The Raman spectra from ambient to 20 GPa are depicted in Fig. 5(a). Five strong Raman modes can be followed during compression. Our previous study showed that these five modes can be assigned as $A_1^{(1)}$, $A_1^{(2)}$, $A_1^{(3)}$, $A_1^{(4)}$, and $A_1^{(5)}$ [42]. Upon pressure increase, the high-frequency modes shift to higher frequency while the lowest mode $A_1^{(1)}$ shifts to lower frequency [Fig. 5(b)]. This negative shift is considered as a common characteristic of the quasicoustic mode among binary and ternary wurtzite semiconductors [43]. The $A_1^{(2)}$ and $A_1^{(3)}$, $A_1^{(4)}$, and $A_1^{(5)}$ cannot be distinguished above 7.5 GPa. Concurrently, a new broad peak emerges at the shoulder of $A_1^{(2)}$, suggesting that a new structure has formed. Above 15 GPa, all the Raman modes disappear, suggesting that the transition to the Raman silent γ -LiGaO₂ is completed. These high-pressure behaviors are consistent with the ADXRD studies.

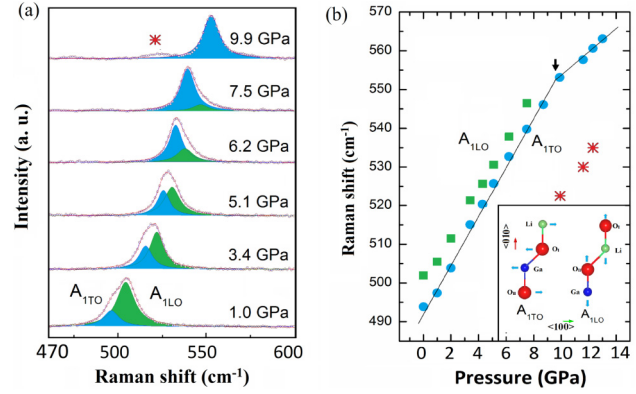


FIG. 6. Evolution of the A_{1TO} and A_{1LO} modes at varying pressures; (a) Lorentzian fits for the A_{1TO} and A_{1LO} modes at different pressures; the red asterisk represents the new peak of the intermediate structure; (b) Raman shift of the A_{1TO} and A_{1LO} modes as a function of pressure; the red asterisks represent the new peak values, associated with the intermediate structure; the inset is the atomic displacement for the two modes in the $\langle 100 \rangle$ and $\langle 100 \rangle$ directions.

The $A_1^{(2)}$ and $A_1^{(3)}$ modes at 494 and 502 cm^{-1} exhibit an interesting behavior, as clearly shown in Fig. 6(a). Below 7.5 GPa, the $A_1^{(2)}$ mode increases its intensity while the $A_1^{(3)}$ mode decreases it. Finally, the $A_1^{(3)}$ mode disappears at 7.5 GPa. A lattice-dynamical study shows that the $A_1^{(2)}$ and $A_1^{(3)}$ modes can be identified as A_{1TO} and A_{1LO} , respectively [39]. In Fig. 6(b), we draw the atomic displacement for $A_1^{(2)}$ and $A_1^{(3)}$. For A_{1TO} , the Li and Ga atoms, and the O_I and O_{II} atoms move in antiphase along the $\langle 100 \rangle$ direction. For A_{1LO} , the Li and Ga atoms all mainly move in phase along the $\langle 010 \rangle$ direction. Also, the O_I and O_{II} atoms move in phase but opposite to the Li and Ga atoms. Upon compression, the distances between the Li and O_I atoms and the Ga and O_{II} atoms get shorter. Therefore, the frequencies of the A_{1TO} and A_{1LO} modes increase with increasing pressure. New bonds form along the $\langle 010 \rangle$ direction above 7.5 GPa as a consequence of the a/b strain increasing, which leads to the disappearance of the related A_{1LO} mode. Thus the A_{1TO} becomes the strongest Raman mode and shows a discontinuity in frequency, which suggests that β -LiGaO₂ transforms into an intermediate structure. Above 11.1 GPa, the PT to γ -LiGaO₂ starts with the structure contracted along the $\langle 001 \rangle$ direction. Finally, the A_{1TO} mode disappears when the PT is completed at 15 GPa.

C. Mechanism of elastic-strain dominated solid-solid PT

We first consider the standard classical analysis of homogeneous coherent nucleation in solids. The transformation criterion for solid-solid PT in elastic materials can be presented as follows [44,45]:

$$\Delta G = (\Delta g_e + \Delta g_v)V + \gamma S \leq 0, \quad (2)$$

where Δg_e is the positive elastic-strain energy per particle volume caused by the transition strain and coherent misfit strain, Δg_v is the negative chemical free-energy density change which is the driving force for the PT, γ is the interfacial free-energy density, V is the volume of the nucleus, and S is the surface area of the nucleus.

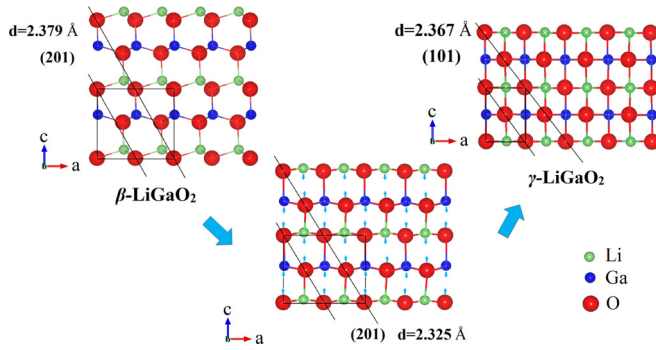


FIG. 7. Mechanism of the structural transformation from β - to γ -LiGaO₂; the small arrows in the intermediate structure show the directions to which the internal atomic coordinates are shifted. The coherent (201) _{β} and (101) _{γ} planes are presented before and after the transition.

For the pressure induced reconstructive PT in β -LiGaO₂, our studies show that the coherent nucleation occurs at the early stage, accompanied with huge microscopic strains. With the nucleus growing, great elastic-strain energy Δg_e is generated due to the big lattice misfits between the nucleus and the parent phase, which in turn inhibits the phase transition. Then the nucleus will be locked at an intermediate structure. With the pressure increasing, Δg_e becomes smaller and the chemical free-energy $|\Delta g_v|$ increases, and then the incoherent nucleation will occur if the elastic strain can be relaxed by the shear stress generated by the transformation strain and/or external stress. In this case, the criterion for solid-solid PT in β -LiGaO₂ can be rewritten as

$$\Delta G = (\Delta g_e - \Delta g_s + \Delta g_v)V + (\gamma_{in} - \gamma_c)S \leq 0, \quad (3)$$

where Δg_s is the positive shear strain energy per particle volume caused by the transition strain and/or external stress, γ_{in} is the incoherent interfacial free-energy density, and γ_c is the coherent interfacial free-energy density.

Now, we present the changes of atomic configuration in β -LiGaO₂ during the PT. Figure 7 shows the positions of the atoms in the initial β -LiGaO₂ structure (left), the intermediate structure (middle), and γ -LiGaO₂ structure just after the transformation (right). There are two necessary strains a/b $\langle 100 \rangle$ and c/b $\langle 001 \rangle$ during the reconstructive PT from β -LiGaO₂ to γ -LiGaO₂. In the early nucleation process, β -LiGaO₂ first undergoes local coherent distortions that bring the oxygen atoms into an appropriate stacking sequence in the (201) plane and form new bonds along the $\langle 010 \rangle$ direction, which leads to the disappearance of the A_{IL0} mode and expanding along the $\langle 100 \rangle$ direction. Then the γ -LiGaO₂ nucleus begins to form

via coherent nucleation based on (101) _{γ} //(201) _{β} . Because the distance of (101) _{γ} is larger than (201) _{β} , they are elastically deformed with respect to what it would be when the other phase was absent; i.e., the (201) _{β} expands and (101) _{γ} contracts. These elastic strains will cause significant elastic-strain energy Δg_e between the nucleus and the parent phase, which will inhibit the growth of the γ -LiGaO₂ nucleus. Therefore, the system stays in the coherent intermediate structure. At higher pressures, when these elastic strains become small enough to be relaxed by the shear stress, the cation and oxygen atoms begin to move in opposite direction and then the γ -LiGaO₂ nucleus grows through incoherent nucleation with the Li atoms and Ga atoms disordered.

IV. SUMMARY

The pressure induced reconstructive PT in β -LiGaO₂ was investigated through *in situ* high-pressure ADXRD and Raman scattering experiments. β -LiGaO₂ transforms into γ -LiGaO₂ at about 11 GPa via an intermediate structure accompanied with significant elastic strain. We propose an elastic-strain dominated mechanism to elucidate the underlying process governing the nucleation and growth in solid-solid reconstructive PT. In the early stage, the new nucleus is formed through coherent distortion. This deformation leads to huge elastic strains with the nucleus growing, which in turn inhibits the phase transition. The elastic strains are too large to be relaxed by the shear stress generated by the transition strain and/or the external stress. As a consequence, an intermediate structure emerges to reduce the elastic strain at the solid-solid phase interface making the transition energetically favorable. At higher pressure, the elastic strain becomes smaller and can be relaxed by shear stress. Then the PT to γ -LiGaO₂ begins and the coherent nucleation is substituted with a semicoherent one with the Li and Ga atoms disordered.

ACKNOWLEDGMENTS

We thank Ignacio Hernandez for helpful discussions. The authors acknowledge support from the National Natural Science Foundation of China (Grants No. 11774247 and No. 11704014), the Science Foundation for Excellent Youth Scholars of Sichuan University (Grant No. 2015SCU04A04), the Research Foundation of Key Laboratory of Neutron Physics (Grant No. 2015BB03), and the Joint Usage/Research Center PRIUS (Ehime University, Japan). The high-pressure ADXRD experiments were supported by the Chinese Academy of Sciences (Grant No. 2017-BEPC-PT-000568).

- [1] Y. Ogawa, D. Ando, Y. Sutou, and J. Koike, *Science* **353**, 368 (2016).
- [2] P. Chowdhury and H. Sehitoglu, *Prog. Mater. Sci.* **88**, 49 (2017).
- [3] O. Tschauer, C. Ma, J. R. Beckett, C. Prescher, V. B. Prakapenka, and G. R. Rossman, *Science* **346**, 1100 (2014).
- [4] T. Irifune, A. Kurio, S. Sakamoto, T. Inoue, and H. Sumiya, *Nature* **421**, 599 (2003).

- [5] R. Z. Khaliullin, H. Eshet, T. D. Kühne, J. Behler, and M. Parrinello, *Nat. Mater.* **10**, 693 (2011).
- [6] H. T. Stokes and D. M. Hatch, *Phys. Rev. B* **65**, 144114 (2002).
- [7] M. Liu and R. A. Yund, *Phys. Earth Planet. Inter.* **89**, 177 (1995).
- [8] M. Kato and T. Fujii, *Acta Mater.* **42**, 2929 (1994).
- [9] S. Limpijumng and W. R. L. Lambrecht, *Phys. Rev. Lett.* **86**, 91 (2001).

- [10] F. Shimojo, S. Kodiyalam, I. Ebbsjö, R. K. Kalia, A. Nakano, and P. Vashishta, *Phys. Rev. B* **70**, 184111 (2004).
- [11] F. P. Bundy, H. M. Strong, H. P. Bovenkerk, and R. H. Wentorf, *J. Chem. Phys.* **35**, 383 (1961).
- [12] M. P. Halsall, P. Harmer, P. J. Parbrook, and S. J. Henley, *Phys. Rev. B* **69**, 235207 (2004).
- [13] P. E. Van Camp, V. E. Van Doren, and J. T. Devreese, *Phys. Rev. B* **44**, 9056 (1991).
- [14] M. Ueno, A. Onodera, O. Shimomura, and K. Takemura, *Phys. Rev. B* **45**, 10123 (1992).
- [15] F. J. Manjón, D. Errandonea, A. H. Romero, N. Garro, J. Serrano, and M. Kuball, *Phys. Rev. B* **77**, 205204 (2008).
- [16] S. E. Boulfelfel, D. Zahn, Yu. Grin, and S. Leoni, *Phys. Rev. Lett.* **99**, 125505 (2007).
- [17] J. S. Wittenberg, T. A. Miller, E. Szilagyí, K. Lutker, F. Quirin, W. Lu, H. Lemke, and A. M. Lindenberg, *Nano Lett.* **14**, 1995 (2014).
- [18] Q. Hu, L. Lei, X. Yan, L. Zhang, X. Li, F. Peng, and D. He, *Appl. Phys. Lett.* **109**, 071903 (2016).
- [19] V. I. Levitas, B. F. Henson, L. B. Smilowitz, and B. W. Asay, *J. Phys. Chem. B* **110**, 10105 (2006).
- [20] X. Yan, D. Tan, X. Ren, W. Yang, D. He, and H. K. Mao, *Appl. Phys. Lett.* **106**, 171902 (2015).
- [21] V. I. Levitas, V. A. Levin, K. M. Zingerman, and E. I. Freiman, *Phys. Rev. Lett.* **103**, 025702 (2009).
- [22] Y. Peng, W. Li, F. Wang, T. Still, A. G. Yodh, and Y. Han, *Nat. Commun.* **8**, 14978 (2017).
- [23] J. D. Eshelby, *Proc. R. Soc. London, Ser. A* **241**, 376 (1957).
- [24] X. Yan, H. Dong, Y. Li, C. Lin, C. Park, D. He, and W. Yang, *Sci. Rep.* **6**, 24958 (2016).
- [25] W. Sailuam, K. Sarasamak, and S. Limpijumngong, *Integr. Ferroelectr.* **156**, 1607 (2014).
- [26] V. F. Britun, A. V. Kurdyumov, and I. A. Petrusha, *Powder Metall. Met. Ceram.* **43**, 87 (2004).
- [27] V. D. Blank, B. A. Kulnitskiy, and A. A. Nuzhdin, *Diamond Relat. Mater.* **20**, 1315 (2011).
- [28] P. Németh, L. A. J. Garvie, T. Aoki, N. Dubrovinskaia, L. Dubrovinsky, and P. R. Buseck, *Nat. Commun.* **5**, 5447 (2014).
- [29] H. K. Mao, J. Xu, and P. M. Bell, *J. Geophys. Res.* **91**, 4673 (1986).
- [30] A. P. Hammersley, S. O. Svensson, M. Hanfland, A. N. Fitch, and D. Hausermann, *High Pressure Res.* **14**, 235 (1996).
- [31] W. Sailuam, K. Sarasamak, M. A. M. Polanco, and S. Limpijumngong, *Ceram. Int.* **43**, S376 (2017).
- [32] M. Marezio, *Acta Crystallogr.* **18**, 481 (1965).
- [33] M. Wang and A. Navrotsky, *J. Solid State Chem.* **178**, 1230 (2005).
- [34] J. C. Anderson and M. Schieber, *J. Phys. Chem. Solids* **25**, 961 (1964).
- [35] L. Lei, T. Irifune, T. Shinmei, H. Ohfuji, and L. Fang, *J. Appl. Phys.* **108**, 083531 (2010).
- [36] See Supplemental Material at <http://link.aps.org/supplemental/10.1103/PhysRevB.97.014106> for the nonhydrostatic compression with NaCl as the pressure transmitting medium.
- [37] F. Birch, *J. Geophys. Res.* **83**, 1257 (1978).
- [38] S. Nanamatsu, K. Doi, and M. Takahashi, *Jpn. J. Appl. Phys.* **11**, 816 (1972).
- [39] A. Boonchun and W. R. L. Lambrecht, *Phys. Rev. B* **81**, 235214 (2010).
- [40] A. K. Singh, A. Jain, H. P. Liermann, and S. K. Saxena, *J. Phys. Chem. Solids* **67**, 2197 (2006).
- [41] K. Momeni, V. I. Levitas, and J. A. Warren, *Nano Lett.* **15**, 2298 (2015).
- [42] L. Lei, H. Ohfuji, J. Qin, X. Zhang, F. Wang, and T. Irifune, *Solid State Commun.* **164**, 6 (2013).
- [43] F. Decremps, J. Pellicer-Porres, A. M. Saitta, J. C. Chervin, and A. Polian, *Phys. Rev. B* **65**, 092101 (2002).
- [44] D. A. Porter and K. E. Easterling, *Phase Transformations in Metals and Alloys*, 2nd ed. (Chapman and Hall, London, 1992).
- [45] J. W. Christian, *The Theory of Transformations in Metals and Alloys*, 2nd ed. (Pergamon, Oxford, UK, 1975).